Proceedings of Montreal 2018
Global Power and Propulsion Forum
7th – 9th May, 2018
www.gpps.global

GPPS-NA-2018-0016

DERIVATION AND NUMERICAL STUDY OF SPRAY BOUNDARY CONDITIONS FOR A PRESSURE SWIRL ATOMIZER ISSUING INTO CO-FLOWING AIR

Benedict Enderle, Felix Grimm, Bastian Rauch, Manfred Aigner
German Aerospace Center (DLR)
Benedict.Enderle@dlr.de
Stuttgart, Germany

Geoffroy Chaussonnet
Institute of Thermal Turbomachinery
Karlsruhe Institute of Technology
Geoffroy.Chaussonnet@kit.edu
Karlsruhe, Germany

ABSTRACT

Newly measured experimental data from detailed measurements of a hollow cone pressure swirl atomizer using simultaneous Phase Doppler Anemometry (PDA) and Laser Doppler Anemometry (LDA) serves as a database for the derivation of spray boundary conditions for multiphase flow simulations. In the experiments the spray is characterized in both quiescent and co-flowing air with an air velocity of $u_g = 36m/s$. Based on the results, a reconstruction strategy for the upstream characteristics of the spray is defined. The resulting spray boundary condition is then investigated by means of Reynolds Averaged Navier Stokes (RANS) simulations and a global sensitivity analysis method. As a result, the necessary calibration factors for the spray boundary condition are reduced and calibrated against the experimental data in quiescent air. Finally, the calibrated boundary condition is used to simulate the experiments in co-flowing air. This approach is found to accurately describe downstream spatial distribution of droplet size and velocity.

INTRODUCTION

Atomization of liquid fuel into a dispersed spray by means of pressure swirl atomizers plays an important role in gas turbine combustor application. Here, resulting spray characteristics and quality strongly affect the fuel distribution and mixing process and thus combustion efficiency, engine performance and finally pollutant formation (Lefebvre, 1998). Therefore, breakup processes and downstream behaviour of dispersed droplets issued from pressure swirl atomizers have been subject to a variety of experimental investigations in the past (Cohen and Rosfjord 1991; Santolaya et al., 2007; Santolaya et al. 2010; Lynch et al., 2011) with most of the experiments focusing on still or slow moving ambient air. However, in applications such as jet stabilized FLOX® based combustors (Gounder et al., 2016) the liquid fuel is injected into a strong co-flow of air which might influence the atomization process as well as the spatial distribution of spray properties.

As pointed out by Fansler (Fansler et al., 2014), numerical simulations of multiphase flows in addition to experiments can help gain a deeper insight into the occurring phenomena and provide additional data which might be difficult to determine in the experiment. In addition, the preliminary design of gas turbine combustors is increasingly built on such simulations. Yet, a major difficulty in the simulation of reacting multiphase flows such as spray injection into a gas turbine combustion chamber is the complexity of the physics at the nozzle exit for both the liquid and the gas phase. This is caused by the complex breakup mechanisms occurring during the disintegration of the liquid jet or sheet into ligaments and finally dispersed droplets. For such simulations, three different strategies may be distinguished: Direct simulation of the primary breakup (Shinjo and Umemura, 2010), modelling of the primary breakup using low order breakup models (Schmidt et al., 1999), or, definition of a spray boundary condition (Quin and Loth, 2016). The first approach is still prohibitive for practical application due to its high computational demand. Breakup models are often limited to specific nozzle types and operating conditions and may require additional calibration of model parameters. In contrast, an accurate

spray boundary condition is able to represent the full spectrum of droplet size and velocity characteristics but requires extensive and accurate input data from experiments.

Therefore, this work is focused on a combined experimental and numerical study of a pressure swirl atomizer where the experiment serves as calibration data for a spray boundary condition which should be able to reproduce both the quiescent as well as the co-flow conditions.

METHODOLOGY

Experimental Apparatus and Measurement Technique

Experimental investigations were conducted on an existing test rig for the characterization of gas turbine atomizers under atmospheric operating conditions. For the present experiments the test rig is extended by a co-flow with a diameter of $d_{cf} = 100\,mm$ as shown in Fig. 1 which allows for the detailed characterization of the spray in quiescent as well as in coaxial flowing air with a co-flow velocity of $U_g = 36\,m/s$. In both cases the ambient and co-flow air has an estimated temperature of $20°\,C$ so that evaporation in the section of interest is minimized.

Three different custom made pressure swirl atomizers are investigated. However, the present work is focused on a hollow cone atomizer with an orifice diameter of $d_0 = 0.28\,mm$ which operates under a fuel pressure of $\Delta p = 16\,bar$ and a fuel mass flow rate of $m_f = 1.75\,g/s$. ShellSol D70 is used as a surrogate for Jet-A1 fuel in the experiments due to the better handling and similar liquid properties relevant for atomization.

For determination of droplet characteristics a commercial Phase Doppler Anemometry (PDA) / Laser Doppler Anemometry system (DANTEC Dynamics Fiber Flow 60X / Dual PDA 57X80) is used. Thus, droplet diameters as well as axial and radial velocity components are measured simultaneously. The laser measurement volume is traversed through the spray cone along r at $z = 0\,mm$ with 13 equidistant measurement points (see coordinate system in Figure 1). Maximum and minimum radial extent of the spray cone is determined from the decay of PDA data rate at the edges of the spray. At each measurement location 50000 valid events are recorded, each of them corresponding to a spherical droplet. Traversal data collection is conducted at two different distances from the atomizer exit with $x = 15\,mm$ and $40\,mm$, respectively. While the first measurement plane allows for a characterization of the spray right after the primary breakup process, the second one aids in validating the defined spray boundary condition in the numerical simulations.

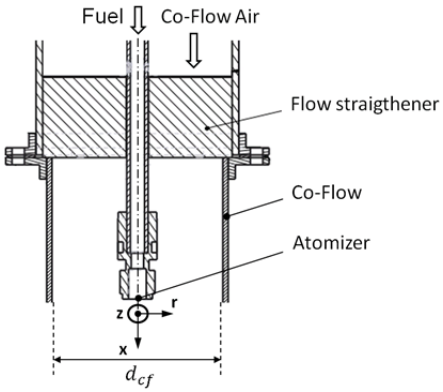

Figure 1 Sketch of the experimental apparatus.

Measurement errors for the droplet velocities are estimated to $\Delta u/u \approx 1.4\%$. Concerning the uncertainty of the diameter, according to the phase ratio validation and the dispersion of the drop size, the order of magnitude of the uncertainty on the SMD is $\pm 1\mu m$.

Numerical Setup

In order to study the reconstruction of spray boundary conditions from experimental data, Reynolds Averaged Navier Stokes (RANS) simulations are performed using the DLR inhouse CFD platform for turbulent reacting multiphase flow simulations THETA-SPRAYSIM (Di Domenico et al., 2011, Eckel et al., 2016) providing an Euler-Lagrange framework using coupled solvers for the gas phase and the liquid phase, respectively. The framework allows for one-way as well as two-way coupled multiphase simulations. In the one-way coupling approach, only influences of the frozen a priori calculated gas field on the dispersed phase are taken into account, whereas two-way coupling also includes feedback of the dispersed phase onto the gas phase by means of an iterative simulation scheme. In the Lagrangian solver, dispersed liquid is tracked by means of computational parcels representing a group of droplets as computing the full scale spray is too computational expensive. In order to permit the post processing of the dispersed phase, tracked particles are registered in arbitrary registration planes across the computational domain

SPRAYSIM enables the definition of flexible spray

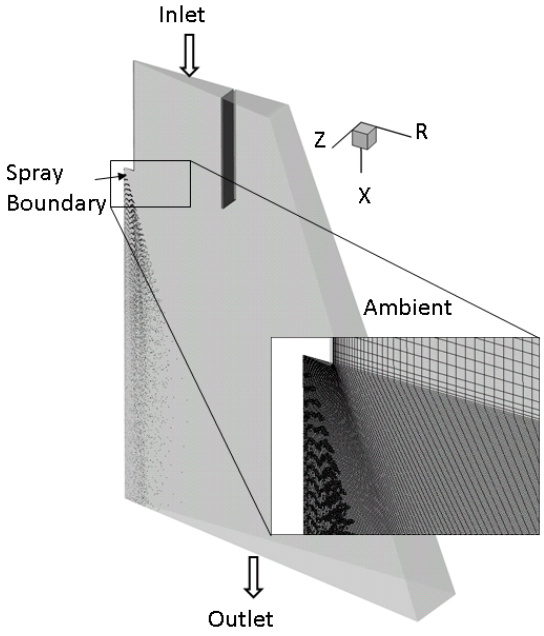

Figure 2 Computational domain with grid detail.

boundary conditions through various droplet size distribution functions and the specification of velocity spectra depending on the droplet size and starting location.

A standard $k-\varepsilon$ Modell is used for the turbulence closure in the RANS simulations. Spray dispersion is modelled by a variant of the Gosman-Ioannides model (Gosman et al., 1983). The computational domain includes the atomizer injection region as well as the co-flow and the ambient but is reduced to a 10 degree wedge due to the rotational symmetry of the geometry and the decrease in computational expense. Although measurements were taken at a maximum distance of $x = 40mm$ downstream of the atomizer, the domain extends up to $x = 300mm$ in order to reduce outflow effects. A sketch of the computational domain is depicted in Fig. 2 including a detail of the grid in the atomizer region. The structured mesh consisted of approximately 57000 cells with a strong clustering in the region of interest. For the ambient, an axial velocity of $u = 0.1\ m/s$ was prescribed for an increased numerical stability.

Spray Reconstruction Strategy

As a general approach for the reconstruction of spray boundary conditions resembling the original atomizer, data from the $x_{PDA} = 15\ mm$ measurement plane is projected further upstream on a boundary condition plane at x_{BC} close to the orifice of the atomizer (see Fig. 3). It is assumed that the disintegration and breakup of the liquid sheet issuing from the atomizer is completed at the boundary condition plane. As a simplification based on the experimental findings, the spray cone in the simulation is assumed to be axially symmetric. Therefore, only experimental data for $r \geq 0\ mm$ is taken into account for the reconstruction. In the boundary condition plane, parcels start from radial starting locations which are projections of the PDA measurement locations. For each starting location, the drop size distribution is specified by means of a Rosin-Rammler distribution function (Lefebvre, 2017)

$$1 - Q_{BC} = \exp(D/X)^q\ , \qquad (1)$$

where Q is the fraction of the total volume contained in drops of diameter less than D and X and q are parameters fitted to the experimental data based on Sauter Mean Diameter (SMD) and Mass Mean Diameter (MMD). Droplet axial and radial velocities $\vec{U}_{BC}(D)$ are specified based on the velocity distribution functions $\vec{U}_{PDA}(D)$ at each corresponding measurement location. In order to compensate the deceleration of droplets in the gasfield after injection, for each droplet size class i a weighting factor kU_i with

$$\vec{U}_{i,BC} = k_{U_i}\,\vec{U}_{i,PDA} \qquad (2)$$

is introduced which needs to be calibrated against the experimental data. In addition, radial shifting of droplet size distribution is accounted for by a weighting factor $kSMD$ with

$$Q(D)_{i,BC} = k_{SMD_i}\,Q(D)_{i,PDA}\ . \qquad (3)$$

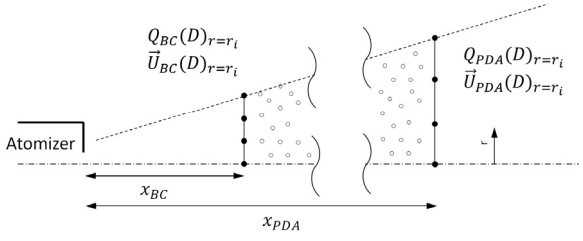

Figure 3 Schematic of spray boundary reconstruction.

RESULTS AND DISCUSSION

Experimental Data

Although mean drop sizes and spray quality of pressure swirl atomizers are largely dependent on operating conditions, empirical correlations allow for an estimation of expected global representative SMD of the spray based on liquid and gaseous properties. The empirical expression of Lefebvre (Lefebvre, 1998) was chosen as a reference,

$$SMD = 2.25\sigma^{0.25}{\mu_L}^{0.25}{\dot{m}_l}^{0.25}{\Delta P_L}^{-0.5}{\varrho_A}^{-0.25}. \qquad (4)$$

Since there is no dependency on ambient air velocity, the estimated SMD for all considered cases reads $SMD_{est.} = 27\ \mu m$. Measured mean SMD and MMD for the two cases are summarized in Tab. 1. They were obtained by weighting the local values at the radial measurement locations i with mass flow rate $\dot{m}_i$ and radius r_i.

$$SMD = \frac{\sum SMD_i A_i \dot{m}_i}{\sum A_i \dot{m}_i}, \quad A_i = \pi(4r_i(r_{i+1} - r_i) \qquad (5)$$

At all positions and operating conditions the measured SMD is well above the one predicted by the empirical correlation. This could be due to the inhomogeneous radial distribution of the SMD and MMD along the real spray as shown later on.

Radial distribution of SMD is displayed in Fig. 4 (a) for the quiescent case at $x = 15mm$ and $x = 40mm$. With further distance to the atomizer exit the SMD increases at the edge of the spray and decreases slightly around the centreline. This characteristic behaviour of hollow cone sprays is caused by the rising entrainment of small droplets in the centreline air core which is accelerated by the hollow cone (Dodge et al, 1984, Chin et al. 1986). In addition, larger droplets tend to penetrate further radial than small ones due to their higher momentum.

Table 1 Measured mean droplet diameters.

$u_g\ [m/s]$	0		36	
$X\ [mm]$	15	40	15	40
$SMD\ [\mu m]$	37.9	39.4	39.1	43.2
$MMD\ [\mu m]$	42.1	42.1	43.5	46.2

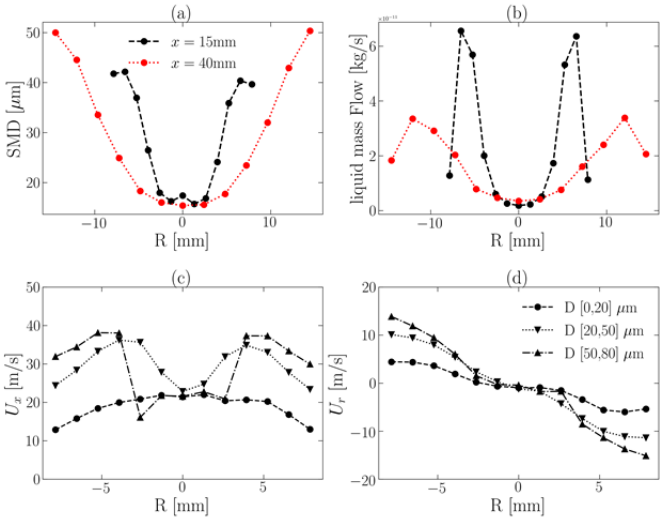

Figure 4 Radial distribution of droplet diameter and velocities for gas velocity $u_g = 0m/s$.

Fig. 4 (b) displays axial liquid mass flow rate for the same case. The sharp rise in the mass flow rate around $r = \pm 5mm$ at $x = 15mm$ axial distance indicates a fully developed hollow cone spray. From the interpolated maxima of flow rate a spray half cone angle of $\theta = 22.5°$ at $x = 15mm$ is computed which reduces to 17° for $x = 40mm$. This could be due to the axial acceleration of droplets by gravity or measurement uncertainties in the determination of mass flow rate.

For the analysis of droplet velocities the droplet spectrum is divided into three size classes with $D_1 < 20\mu m$, $20\mu m \leq D_2 < 50\mu m$ and $50\mu m \leq D_3$, each of them representing roughly a third of the overall liquid mass flow based on the mass weighted cumulative size distribution of the droplet spectrum. Axial and radial velocities over the radial extent of the spray at $x = 15mm$ is plotted in Fig. 4 (c) and (d), respectively. Large droplets of class D_3 and D_2 reach almost twice the velocity in both axial and radial direction compared to small droplets of class D_1. This is

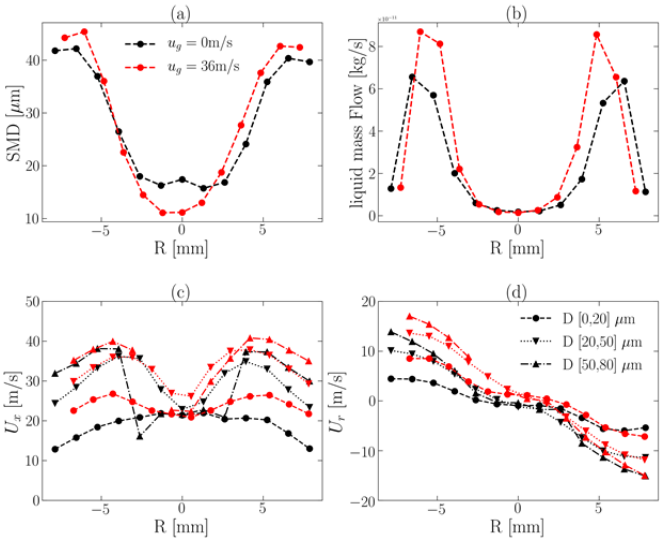

Figure 5 Comparison of droplet diameter and velocity for $u_g = 0m/s$ and $u_g = 36m/s$.

caused by the effect that large droplets maintain the high velocity of the liquid sheet after primary atomization while small droplets tend to couple to the lower local induced airflow (Sommerfeld, 1998). The highest axial velocity of large droplets is connected to the region of maximum mass flow and therefore the outer region of the hollow cone.

Influence of Co-Flow

In order to study the effect of co-flowing air on droplet sizes and velocities experimental data for the quiescent air case is compared with the results from the co-flow case at $x = 15mm$. In figure xyz the local SMD around $R = 0mm$ clearly decreases for the co-flow case which might be a consequence of elevated entrainment of small droplets in the inner air core. However, looking at the overall weighted SMD in Tab. 1 there is no improvement in atomization due to the co-flowing air since both SMD and MMD marginally increment in the presence of the co-flow. Based on the maxima of liquid mass flow rate in Fig. 5 (b) a slightly lower half cone angle of $\theta = 20°$ compared to the quiescent operating conditions is calculated, indicating a narrowing of the spray cone due to the co-flow.

The velocity profiles in Fig. 5 (c) and (d) show a similar shape for both cases. However, small droplets of class D_1 demonstrate a strong influence of the co-flow on maximum velocities with a gain of up to $10m/s$ in axial velocity while larger droplet are less affected due to their higher response time.

The present measurements provide a consistent and extensive validation database for the simulation and numerical study of pressure swirl atomizer under different co-flow conditions.

Numerical Simulation

In a first study the one way and two way coupling approaches aree compared for the $u_g = 0m/s$ case using the same estimated spray boundary condition for both simulation strategies. The resulting axial velocity at $x = 15mm$ downstream of the atomizer for droplet size classes as defined in the previous section is shown in Fig. 6. Strong deceleration of droplets is present in the one way coupled results. Especially the smallest droplets are almost stagnant. As a consequence of the one way coupling approach the frozen quiescent gasfield is not able to accelerate in the presence of the expanding spray. Therefore, the inner air core in the hollow cone cannot evolve and is not reproduced. The resulting high relative velocity between the moving droplets

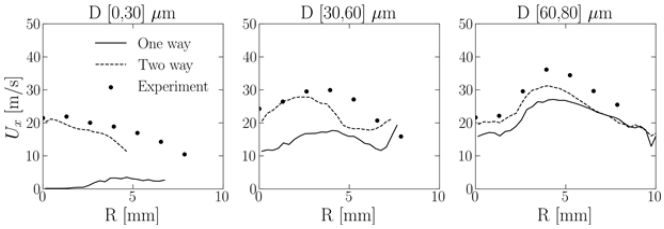

Figure 6 Axial droplet velocity from one and two way coupling simulations.

Table 2 Parameter range for MOAT analysis.

	k_{U1} [-]	k_{U2} [-]	k_{U3} [-]	k_{SMD} [-]
Min.	1	1	1	0.9
Max.	1.5	1.5	1.5	1.1

and the stationary gasphase leads to a strong damping of droplet motion. An increased starting velocity at the boundary plane in the one way coupled simulation in order to match the experimental data would lead to unphysical velocities for the small droplets. Based on these findings all numerical results in the following are carried out with two way coupled simulations.

Sensitivity Analysis

To match the experimental data weighting factors for velocity classes and droplet diameters at the spray boundary condition were introduced. For a better understanding of the effect of these weighting factors on the downstream structure of the spray and a potential reduction in calibration factors a systematic sensitivity analysis was performed. In order to reduce the required number of simulations the Morris-One-At-A-Time (MOAT) (Morris, 1991) screening method for global sensitivity analysis was chosen. In this method, input parameters are varied one at a time while the afore changed parameter remains at the changed value. The computed model response is then compared to the response before the variation and the next parameter is changed until all parameters are altered. By repeating this procedure multiple times - with p being the number of repetitions - statistical moments of resulting elementary effects are derived. Here, first order moments (mean σ) indicate the overall effect of a model input on the simulation output while second moments (standard deviation μ) imply nonlinear effects or interactions among different input parameters. This renders a very efficient routine compared to more demanding methods for sensitivity analysis (Saltelli, 2004).

A MOAT study with $p = 5$ was conducted for the $u_g = 0m/s$ case using parameter ranges as listed in Tab. 2. As a simplification, constant calibration factors over all radial starting positions were assumed. The model response was defined as the Root Mean Squared (RMS) deviation between experiment and simulation over all N radial measurement positions i at $x = 15mm$,

$$U_{RMS} = \sqrt{\frac{1}{N}\sum(U_{Exp.,i} - U_{Sim,i})^2} \quad (6)$$

and

$$SMD_{RMS} = \sqrt{\frac{1}{N}\sum(SMD_{Exp.,i} - SMD_{Sim,i})^2}\,. \quad (7)$$

Data in Fig. 7 is displayed as mean and standard deviation of elementary effects for the axial velocity in the three size classes and the SMD. Thus, influence of the

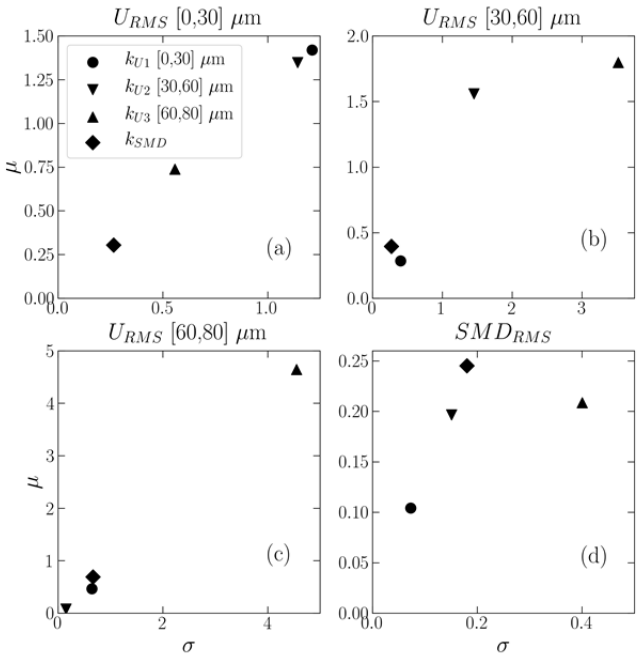

Figure 7 Elementary effects from MOAT analysis

weighting factors can be divided into effects on the small (Fig. 7 (a)), medium (Fig. 7 (b)) and large (Fig. 7 (c)) droplets as well as on the SMD (Fig. 7 (d)). As evident from the figure the calibration factor for size class D_3 causes strong linear and interaction effects for size classes D_2 and D_3 and even the SMD (Fig. 7 (c-d)). This indicates a major interaction between the large droplets and the gas phase by means of an acceleration of the gas field which is then fed back to the smaller droplets in the dispersed phase. On the other hand, from the MOAT plot of size class D_3 (Fig. 7 (c)) it is concluded that small droplets are not able to affect the velocity of large droplets. Moreover, there is only a minor effect of the SMD calibration factor k_{SMD} on the droplet velocities and even the variation in SMD is more driven by the change in large droplet velocity due to a resulting redistribution of droplets after injection (Fig. 7 (d)).

Due to this result only the calibration factors for velocity components are calibrated in the following while the SMD distribution is kept constant at the experimental values.

Calibration for quiescent air case

Calibration of weighting factors based on the experimental results for $u_g = 0m/s$ at $x = 15mm$ was

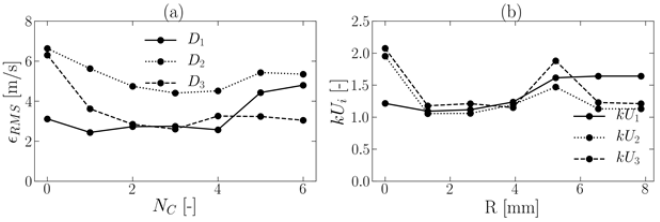

Figure 8 Residuals and weighting factors from calibration

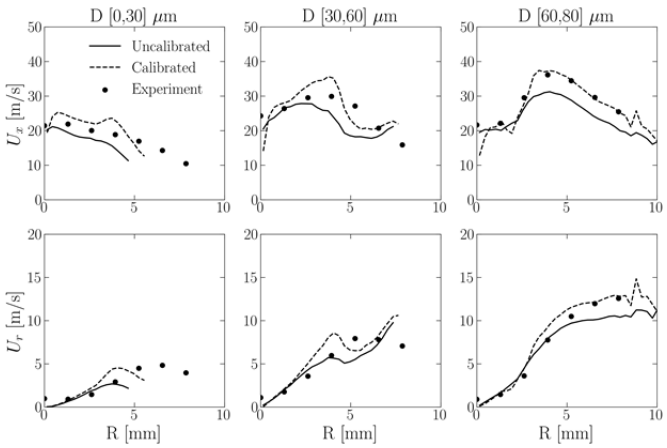

Figure 9 Axial and radial droplet velocity before and after calibration.

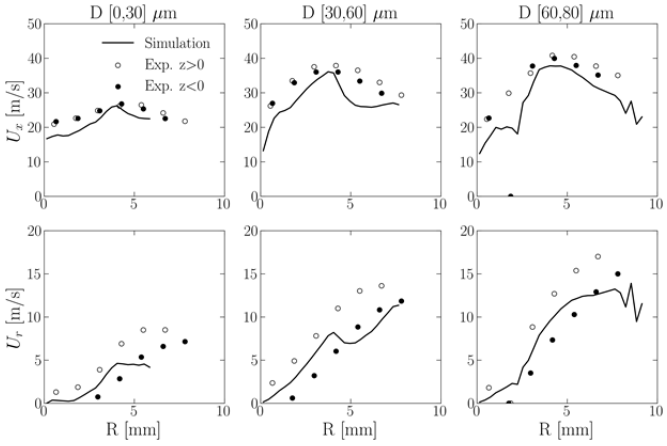

Figure 11 Axial and radial droplet velocity at $x = 15mm$ for $u_g = 36m/s$.

performed using a simplified iterative scheme obtained from the definition of weighting factors in Eq. (2). For calibration step $n+1$ the weighting factors are calculated by

$$kU_i^{n+1} = \frac{U_{Exp.,i}}{U_{Sim.,i}^n}, \quad kU_i^0 = 1. \tag{8}$$

Ten consecutive calibration simulations were run. Fig. 8 (a) shows the progression of RMS deviation between experiment and calibration (see Eq. (5) and (6)) over the simulations. The minimum deviation and therefore the best fit is found at iteration $n = 3$. Resulting radial distribution of weighting factors is given in Fig. 8 (b). For all size classes weighting factors peak at the centreline and in the region of the spray cone around $R = 5mm$. Highest factors - and therefore additional acceleration at the spray boundary - are required for the large droplets which is consistent with the findings from the MOAT analysis where they demonstrated the strongest influence on the dispersed phase.

A comparison between the uncalibrated and calibrated results is shown in Fig. 9 for axial and radial velocities. After calibration the simulations are in good agreement with the experimental data. The velocity profile of the large droplets is excellently met whereas axial velocities of medium and small droplets are slightly overestimated by the simulation. As evident from Fig. 10, SMD and MMD are reproduced well by the simulation up to a radius of approximately $R = 6mm$ with the exception of the centreline region where both SMD and MMD are underestimated. For the outer region of the spray, high values of characteristic diameters are predicted which is a consequence of poor statistic in this region. This is caused by the fact that only few computational parcels are registered in this region.

Simulation of Co-Flow case

Using the calibrated spray boundary condition from the previous section, the case with a co-flow velocity of $u_g = 36m/s$ was simulated without any further calibration. This was motivated by the finding in the experiment that in the case considered the co-flow had only minor influence on the primary atomization. All resulting changes in droplet velocities and characteristic diameters compared to the quiescent case should be a result of droplet gasfield interaction.

Simulation results for axial and radial velocity components are given in Fig. (11). Note that experimental results for $r > 0mm$ as well as $r < 0mm$ are included for comparison as they revealed a slight asymmetry in the experiments. Although the shape of the profiles is in very good agreement with the experimental data the simulation results in a minor underestimation of the velocity components. As illustrated in Fig. 12, SMD and MMD are well predicted with the same deviation at the outer region as in the quiescent case due to poor registration statistics.

Thus, the simulation is able to reproduce all effects of coaxial co-flow on the droplets using a spray boundary condition which is calibrated against data from quiescent measurements.

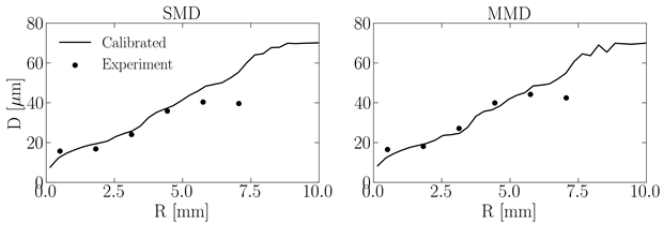

Figure 10 Computed characteristic diameters at $x = 15mm$ after calibration.

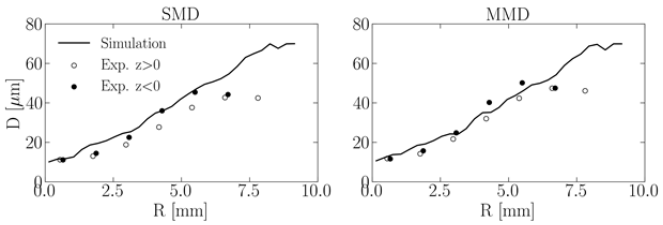

Figure 12 Characteristic diameter at x = 15mm for $u_g = 36m/s$

CONCLUSIONS

An experimental and computational study on pressure swirl atomizers issuing into quiescent and co-flowing air was conducted. In the experiments spray characteristics typical for such an atomizer were identified and showed agreement with findings from previous studies. It was found that in the case considered the co-flow had no influence on the primary atomization. However, effects due to droplet acceleration and redistribution in the presence of the co-flow were found. The measurement data acquired provides a validation database for further numerical studies on pressure swirl atomizer under various conditions.

A spray reconstruction strategy for the definition of a spray boundary condition close to the atomizer exit was defined. The MOAT sensitivity analysis revealed that large droplets have a major influence on the velocity of smaller droplets via gas phase coupling. A boundary condition for the quiescent air case was successfully calibrated against the experimental data. Using the same boundary condition the co-flow case was successfully simulated resulting in excellent agreement with the experimental data. Thus, a spray boundary condition based on quiescent data is able to predict the behaviour of sprays in co-flowing air, a use case which is found for example in gas turbine combustors.

Furthermore, it is concluded that the reconstruction and calibration strategy as described provides useful boundary conditions for the simulation of pressure swirl atomizers.

NOMENCLATURE

Abbreviations

BC	Boundary Condition	[-]
CF	Co-Flow	[-]
CFD	Computational Fluid Dynamics	[-]
FLOX	Flameless Oxidation	[-]
LDA	Laser Doppler Anemometry	[-]
MMD	Mass Mean Diameter	$[m]$
MOAT	Morris-One-At-A-Time	[-]
PDA	Phase Doppler Anemometry	[-]
RANS	Reynolds Averaged Navier Stokes	[-]
RMS	Root Mean Square	[-]
SMD	Sauter Mean Diameter	$[m]$

Variables (Latin)

D	Droplet diameter	$[m]$
d_{CF}	Diameter of Co-Flow	$[m]$
d_0	Atomizer orifice diameter	$[m]$
k_U	Velocity calibration factor	[-]
k_{SMD}	SMD calibration factor	[-]
$\dot{m}_f$	Fuel mass flow rate	$[kg/s]$
n	Calibration step	[-]
N	Number of radial positions	[-]
p	Pressure	$[Pa]$
q	Rosin Rammler dispersion factor	[-]
Q	Volume fraction	[-]
U, U_g	Velocity, gas velocity	[-]
x, r, z	Spatial coordinates	$[m]$

Variables (Greek)

Δ	Difference	[-]
ε	Dissipation rate	$[m^2/s^3]$
κ	Turbulent kinetic energy	$[m^2/s^2]$
μ	Standard deviation	[-]
σ	Mean	[-]
ϱ	Density	$[kg/m^3]$
θ	Spray half cone angle	[°]

ACKNOWLEDGMENTS

The authors would like to thank Teresa Siebel for her support during the preparation of the measurements.

REFERENCES

[1] Lefebvre, Arthur H. (1998): Gas turbine combustion. CRC press.

[2] Cohen, J. M., and T. J. Rosfjord (1991): "Spray patternation at high pressure." Journal of Propulsion and Power 7.4: 481-7.

[3] Santolaya, J. L., et al. (2007): "Experimental study of near-field flow structure in hollow cone pressure swirl sprays." Journal of propulsion and power 23.2: 384-391.

[4] Santolaya, J. L., et al. (2010): "Analysis by droplet size classes of the liquid flow structure in a pressure swirl hollow cone spray." Chemical Engineering and Processing: Process Intensification 49.1: 125-131.

[5] Lynch, Amy, et al. (2011): "Spray characteristics of a pressure-swirl fuel injector subjected to a crossflow and a coflow." Atomization and Sprays 21.8

[6] Gounder, James D., et al. (2016): "Experimental and numerical investigation of spray characteristics in a new FLOX® based combustor for liquid fuels for Micro Gas Turbine Range Extender (MGT-REX)." Proceedings. 52nd AIAA/SAE/ASEE Joint Propulsion Conference 2016

[7] Fansler, Todd D., and Scott E. Parrish. (2014): "Spray measurement technology: a review." Measurement Science and Technology 26.1: 012002

[8] Shinjo, J., and A. Umemura. (2010): "Simulation of liquid jet primary breakup: dynamics of ligament and droplet formation." International Journal of Multiphase Flow 36.7: 513-532.

[9] Schmidt, David P., et al. (1999): „Pressure-swirl atomization in the near field." No. 1999-01-0496. SAE Technical Paper.

[10] Qin, C., and E. Loth (2016): "Numerical description of a pressure-swirl nozzle spray." Chemical Engineering and Processing: Process Intensification 107: 68-79.

[11] Di Domenico, et al. (2011): "Numerical simulations of confined, turbulent, lean, premixed flames using a detailed

chemistry combustion model." Proceedings of ASME Turbo Expo. 2011.
[12] Eckel, Georg, et al. (2016): "Semi-empirical model for the unsteady shear breakup of liquid jets in cross-flow." Atomization and Sprays 26.7
[13] Gosman, A. D., and E. Loannides. (1983): "Aspects of computer simulation of liquid-fueled combustors." Journal of Energy 7.6: 482-490.
[14] Lefebvre, Arthur H., and Vincent G. McDonell. (2017): Atomization and sprays, CRC press, 2017
[15] Sommerfeld, M. (1998): "Analysis of isothermal and evaporating turbulent sprays by phase-Doppler anemometry and numerical calculations." International journal of heat and fluid flow 19.2: 173-186.
[16] Morris, Max D. (1991): "Factorial sampling plans for preliminary computational experiments." Technometrics 33.2: 161-174.
[17] Saltelli, Andrea, et al. Sensitivity analysis in practice: a guide to assessing scientific models. John Wiley & Sons, 2004.